Effect of Al2O3 Recombination Barrier Layers Deposited by Atomic Layer Deposition in Solid-State CdS Quantum Dot-Sensitized Solar Cells

ARTICLE *in* THE JOURNAL OF PHYSICAL CHEMISTRY C · FEBRUARY 2013

Impact Factor: 4.77 · DOI: 10.1021/jp311846r

8 AUTHORS, INCLUDING:

Thomas Brennan
Stanford University
16 PUBLICATIONS **431** CITATIONS
SEE PROFILE

Colin D. Bailie
Stanford University
12 PUBLICATIONS **341** CITATIONS
SEE PROFILE

Eric T Hoke
Stanford University
43 PUBLICATIONS **1,881** CITATIONS
SEE PROFILE

Stacey Bent
Stanford University
230 PUBLICATIONS **5,349** CITATIONS
SEE PROFILE

THE JOURNAL OF PHYSICAL CHEMISTRY C

Article

pubs.acs.org/JPCC

Effect of Al_2O_3 Recombination Barrier Layers Deposited by Atomic Layer Deposition in Solid-State CdS Quantum Dot-Sensitized Solar Cells

Katherine E. Roelofs,[†] Thomas P. Brennan,[‡] Juan C. Dominguez,[‡] Colin D. Bailie,[†] George Y. Margulis,[†,§] Eric T. Hoke,[†,§] Michael D. McGehee,[†] and Stacey F. Bent*[,‡]

[†]Department of Materials Science and Engineering, Stanford University, Stanford, California 94305, United States

[‡]Department of Chemical Engineering, Stanford University, Stanford, California 94305, United States

[§]Department of Applied Physics, Stanford University, Stanford, California 94305, United States

Supporting Information

ABSTRACT: Despite the promise of quantum dots (QDs) as a light-absorbing material to replace the dye in dye-sensitized solar cells, quantum dot-sensitized solar cell (QDSSC) efficiencies remain low, due in part to high rates of recombination. In this article, we demonstrate that ultrathin recombination barrier layers of Al_2O_3 deposited by atomic layer deposition can improve the performance of cadmium sulfide (CdS) quantum dot-sensitized solar cells with spiro-OMeTAD as the solid-state hole transport material. We explored depositing the Al_2O_3 barrier layers either before or after the QDs, resulting in $TiO_2/Al_2O_3/QD$ and $TiO_2/QD/Al_2O_3$ configurations. The effects of barrier layer configuration and thickness were tracked through current−voltage measurements of device performance and transient photovoltage measurements of electron lifetimes. The Al_2O_3 layers were found to suppress dark current and increase electron lifetimes with increasing Al_2O_3 thickness in both configurations. For thin barrier layers, gains in open-circuit voltage and concomitant increases in efficiency were observed, although at greater thicknesses, losses in photocurrent caused net decreases in efficiency. A close comparison of the electron lifetimes in TiO_2 in the $TiO_2/Al_2O_3/QD$ and $TiO_2/QD/Al_2O_3$ configurations suggests that electron transfer from TiO_2 to spiro-OMeTAD is a major source of recombination in ss-QDSSCs, though recombination of TiO_2 electrons with oxidized QDs can also limit electron lifetimes, particularly if the regeneration of oxidized QDs is hindered by a too-thick coating of the barrier layer.

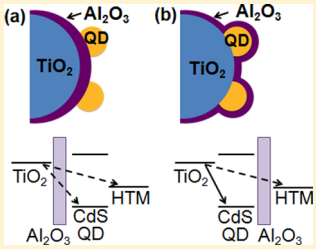

INTRODUCTION

Dye-sensitized solar cells (DSSCs) offer a compelling low-cost alternative to conventional photovoltaic cells. The DSSC architecture consists of a mesoporous film of a wide-band-gap oxide, such as TiO_2 or ZnO, coated with a monolayer of dye molecules.[1] The pores are filled with a redox electrolyte that regenerates dye molecules that have injected an excited electron into the metal oxide photoanode. DSSCs have recently reached power conversion efficiencies of over 12%, by cosensitization of two donor−π-bridge−acceptor dyes.[2] In the search for new approaches to increase efficiency and device stability, a number of studies have investigated replacing the sensitizing dye with semiconductor quantum dots (QDs), creating quantum dot-sensitized solar cells (QDSSCs).[3−8] The size quantization of QDs[9] allows for precise control over the band gap for optimal absorption and over band offsets for optimal charge transfer. In particular, QDs can be tuned to absorb in the near-IR, which is difficult to achieve with dyes, and QDs can exhibit higher absorption cross sections than organic or metal−organic dyes over a broad spectral range.[10,11] QDs can be grown directly on the mesoporous TiO_2 by chemical bath deposition,[12,13] successive ion layer adsorption and reaction (SILAR),[14,15] electrodeposition,[16] or atomic layer deposition (ALD).[17,18]

Commercialization of DSSC technology has generated interest in employing solid-state hole-transport materials (HTMs), such as the commonly used spiro-OMeTAD (2,2′,7,7′-tetrakis-(*N*,*N*-di-*p*-methoxyphenylamine)-9,9′-spirobifluorene), to replace the liquid electrolyte.[19] The use of solid-state HTMs avoids the problem of electrolyte leakage and corrosion of metal contacts, and aims to improve long-term stability. Unfortunately, the recombination rate of electrons in TiO_2 with holes in spiro-OMeTAD is higher than the analogous pathway with the standard I^-/I_3^- liquid electrolyte.[20] The high recombination rate limits the active layer thickness in solid-state devices to ∼2 μm, due to the consequently low charge carrier diffusion lengths as well as further increases in recombination rate at greater thicknesses from poor pore-filling by spiro-OMeTAD.[21−23] Active layers of TiO_2 coated with dye molecules must reach thicknesses of ∼10 μm to absorb all incident light; thus solid-state DSSC efficiencies are limited by insufficient light absorption. The high absorption cross section of QDs, with the potential to absorb strongly in a limited

Received: December 2, 2012
Revised: February 20, 2013
Published: February 25, 2013

thickness, makes QDs especially suitable for use in solid-state devices.

To reduce recombination in DSSCs, the deposition of thin layers of metal oxides at the TiO_2 interface has been explored. For the current work, ALD was chosen to deposit barrier layers of Al_2O_3, due to the ability of ALD to introduce high-quality, conformal films on high aspect ratio surfaces, with angstrom-level control of film thickness, and excellent uniformity over large areas.[24] In DSSCs, metal oxide barrier layers are deposited on TiO_2 before the dye and, in this position, can detrimentally interfere with charge injection from the dye into the TiO_2 photoanode.[25] In QDSSCs, there is the possibility to deposit barrier layers after the QDs, due to the higher temperature and physical stability of QDs compared to dyes. While there has been recent progress in developing low-temperature ALD for deposition of barrier layers after dye molecules in DSSCs,[26] temperature constraints still greatly limit material choice. Previous reports of surface coatings in QD-sensitized devices were conducted in cells with liquid electrolytes, with the intent of protecting the QDs from corrosion by the electrolyte, passivating QD surface defects, or increasing the adsorption of cosensitized dyes.[27−30]

In this work, Al_2O_3 barrier layers of varying thicknesses are deposited in solid-state CdS QDSSCs before and after the QDs (Figure 1), with spiro-OMeTAD as the HTM. Cadmium

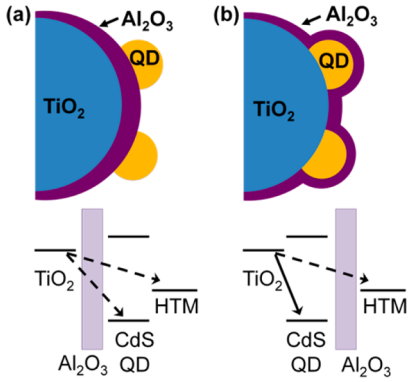

Figure 1. Schematic of barrier layer configurations (not to scale) available in quantum dot-sensitized solar cells: (a) $TiO_2/Al_2O_3/QD$ and (b) $TiO_2/QD/Al_2O_3$, resulting, respectively, from deposition of the Al_2O_3 layer before and after the CdS QDs. Spiro-OMeTAD is employed as the hole-transport material (HTM). Arrows indicate undesirable recombination pathways; pathways that may be blocked by the Al_2O_3 barrier layer are shown by dashed arrows.

sulfide was chosen as the QD material due to its ease of deposition by SILAR and as the large band gap of CdS ensures electron injection into the TiO_2 conduction band for any QD size. This study takes advantage of the flexibility of barrier placement that the QDSSC system offers to optimize device performance and better understand the recombination processes limiting QDSSC device efficiency. As shown in the energy diagrams of Figure 1, in both the resulting $TiO_2/Al_2O_3/QD$ and $TiO_2/QD/Al_2O_3$ configurations, Al_2O_3 blocks recombination from TiO_2 to spiro-OMeTAD, and in the $TiO_2/Al_2O_3/QD$ configuration, Al_2O_3 also blocks recombination from TiO_2 to oxidized QDs. In both configurations, however, the barrier layer can also interfere with charge separation steps necessary for photocurrent collection: either electron injection into TiO_2 or hole transfer to spiro-OMeTAD. Thus, optimization rests on the concept of "kinetic redundancy", in which the desirable charge-transfer step is much faster than the competing undesirable step, such as in the case of electron injection into TiO_2, which occurs at a much faster rate than the competing undesirable decay of the excited electron within the QD.[31] In such a situation, the insertion of a barrier layer could slow electron injection without appreciably affecting the electron injection yield, allowing for devices to benefit from decreased recombination without detrimental effects on photocurrent collection. In the QDSSC system, there is the opportunity to place the barrier layer such that it slows whichever charge separation step has the greatest kinetic redundancy, electron injection or hole transfer to spiro-OMeTAD.

The effects of barrier layer thickness and position were tracked through current−voltage measurements of device performance and transient photovoltage measurements of electron lifetimes. For the Al_2O_3 ALD system employed in this paper, less than a monolayer of Al_2O_3 is deposited per cycle on the TiO_2 surface.[25,32,33] Thus, while ALD allows for the growth of ultrathin Al_2O_3 layers, one Al_2O_3 ALD cycle results in incomplete coverage of the TiO_2 surface, and for the low cycle numbers used in this study ($\lesssim$5), the spatial variation in film thickness is considerable compared to the total film thickness.[25]

EXPERIMENTAL SECTION

Mesoporous TiO_2 Substrates. Except for the sensitization steps, solid-state QDSSCs were fabricated similarly to the procedure for solid-state DSSCs described elsewhere.[34] For the transparent electrode, glass substrates coated with fluorine-doped tin oxide (15 Ω/□, Pilkington) were patterned by etching with 4 M HCl and Zn. Substrates were then coated with a thin (∼50 nm) compact layer of TiO_2 by aerosol spray pyrolysis at 450 °C using air as a carrier gas. The mesoporous TiO_2 layer was then deposited by doctor-blading a commercial paste of 20 nm diameter anatase TiO_2 particles (Dyesol 18-NRT) diluted with terpineol. The films were annealed at 450 °C, resulting in a film thickness of ∼2.2 μm as measured by a Dektak profilometer. The mesoporous TiO_2 films were immersed overnight in a 0.02 M aqueous $TiCl_4$ solution, and then annealed again at 450 °C.

SILAR of CdS QDs. Cadmium sulfide QDs were grown on mesoporous TiO_2 substrates by the SILAR process at room temperature. To complete a SILAR cycle, substrates were first dipped in a 0.1 M $CdSO_4$ aqueous solution for 5 min. They were then rinsed in DI water and dipped in a 0.1 M Na_2S aqueous solution for 5 min.[14,15] We found previously that maximum device efficiency was achieved when CdS QD growth was stopped at 6 SILAR cycles,[15] so all devices reported in this work were fabricated with 6 CdS SILAR cycles. As characterized in previous work from Tauc Analysis of UV−vis absorption spectra of QD-sensitized mesoporous TiO_2 substrates, CdS QDs deposited by 6 SILAR cycles exhibit band gaps of 2.5−2.8 eV.[15] By comparison with known values in the literature, these band-gap values correspond to CdS QD sizes of 3−5 nm in diameter.[35] For devices where the Al_2O_3 barrier layer was deposited before the QDs, a buffered Na_2S solution was used, to avoid etching of the Al_2O_3 layer. Specifically, the 0.1 M Na_2S aqueous solution was buffered with an ammonium chloride/ammonium hydroxide solution to reach a pH of 9. UV−visible spectroscopy confirmed that CdS QDs produced by the buffered SILAR process were optically identical to those produced by the unbuffered process.

dx.doi.org/10.1021/jp311846r | J. Phys. Chem. C 2013, 117, 5584−5592

ALD of Al_2O_3. ALD of Al_2O_3 was performed in a custom-built, traveling-wave, hot wall, tube furnace-type reactor with five radially oriented precursor manifolds. The substrate temperature was maintained at 175 °C during ALD. The precursors, trimethylaluminum (TMA) (Sigma-Aldrich) and water, were held at room temperature. N_2 was used as a carrier and purge gas. To ensure that the precursors were able to sufficiently penetrate the mesoporous substrate, a soak step (when the reaction chamber is isolated from the vacuum pump and the precursor manifold valve is closed) was employed, similar to that adopted by Lin et al.[33] First, TMA was pulsed for 5 s and allowed to soak for an additional 40 s; after this, the chamber was evacuated for 70 s (purge step). Next, H_2O was pulsed for 3 s and allowed to soak for an additional 40 s, followed by a 70 s purge step. The growth rate of this process over 100 cycles on a Si(100) wafer (Silicon Quest) with a native oxide as measured by a spectroscopic ellipsometer (Woollam Alpha SE) was ∼1.6 Å/cycle. This process was previously shown, by Auger electron spectroscopy of TiO_2 layer cross sections, to deposit Al_2O_3 through the entire thickness of the mesoporous TiO_2 substrate.[25]

The stability of the Al_2O_3 layer in the buffered SILAR process was confirmed by tracking the etching rate of a thick planar film (100 ALD cycles) of Al_2O_3 deposited on a planar Si(100) wafer, submersed in the buffered Na_2S solution. The etching rate was determined by spectroscopic ellipsometry to be 0.2 ± 0.1 Å/h. As the Al_2O_3-coated mesoporous TiO_2 substrates were submersed in the Na_2S solution for less than 30 min throughout the entire SILAR process, a negligible amount of the Al_2O_3 layer will be etched.

Active Layer Characterization. A Cary 6000i UV−visible spectrometer (Varian) was used to characterize the optical properties of the active layer. For these studies, mesoporous TiO_2 was deposited on glass microscope slides, and treated with the desired combination of SILAR and ALD cycles.

To study the growth of Al_2O_3 on TiO_2 and CdS surfaces, X-ray photoelectron spectroscopy (XPS) measurements were taken with a PHI 500 VersaProbe Scanning XPS Microprobe equipped with an Al Kα 1486 eV radiation source at a pressure of 6×10^{-10} Torr. To fabricate the TiO_2 surfaces, thick planar films (∼8 nm) of anatase TiO_2 were deposited by ALD on Si(100) wafers, as described in previous work.[15] For the CdS surface, thick planar films of CdS were deposited by SILAR (150 cycles) on Si(100) wafers. Al_2O_3 was then grown by ALD on the TiO_2 and the CdS films. The Al_2O_3 growth was tracked with high-resolution XPS scans of the Al (2p), Ti (2p), and Cd (3d) peaks, taken at a pass energy of 23.5 eV and a resolution of 0.1 eV/step, at multiple spots on the surface.

Device Fabrication. For the TiO_2/Al_2O_3/QD devices, mesoporous TiO_2 substrates were subjected first to ALD of Al_2O_3, then to the buffered SILAR process. For the TiO_2/QD/Al_2O_3 devices, mesoporous TiO_2 substrates first underwent the unbuffered SILAR process, then underwent ALD of Al_2O_3. The QD-sensitized control substrates (0 ALD cycles) used for comparison with the TiO_2/QD/Al_2O_3 devices were heated to 175 °C to account for any effects the heat treatment involved in the ALD process might have on the QDs. As described elsewhere,[34] the solution of the solid-state hole-transporting material was composed of 225 mg mL^{-1} of spiro-OMeTAD (Lumtec) dissolved in chlorobenzene, with *tert*-butylpyridine added at a ratio of 1:10.3 μL/mg of spiro-OMeTAD, and lithium bis-(trifluoromethylsulfonyl)imide salt (170 mg mL^{-1} in acetonitrile) added at a ratio of 1:4.8 μL/mg of spiro-OMeTAD. A small amount of the spiro-OMeTAD solution (30 μL for 3.75 cm^2 substrates) was deposited onto the TiO_2 substrates at room temperature, and spin-coated at 2000 rpm for 30 s. Finally, 200 nm thick Ag counter electrodes were deposited by thermal evaporation under vacuum below 10^{-6} Torr. Final device areas were on the order of 0.1 cm^2. Devices were stored inside a desiccator prior to electrical measurements.

Electrical Measurements. For photovoltaic measurements, an AM 1.5 solar simulator (Oriel 91160) equipped with a 300 W ozone-free Xe arc lamp (6258) was used. The lamp was calibrated to 1 sun (100 mW cm^{-2}) using a reference NREL calibrated Si photodiode equipped with an IR cutoff filter. Current−voltage (J−V) curves were collected with a Keithley 2400 SourceMeter, with a sweep delay of 40 ms. Devices were light-soaked until maximum efficiencies were reached (up to 1 h). Transient photovoltage measurements were conducted using a setup described in greater detail elsewhere.[23,36] Briefly, devices were white-light-biased at 1 sun with an array of white LEDs (Lumiled) and pulsed with a square wave from a white LED (∼0.05 suns). A given device was held at constant current with a 2400 Keithley SourceMeter, biasing the device to a specific point on its J−V curve, and the decay of the increased photovoltage from the light pulse was collected at various bias points. The ∼0.05 sun light pulse length was set to 50, 100, or 500 ms, depending on the time necessary to sufficiently capture the photovoltage decay. The monoexponential photovoltage decay was fit to extract a recombination lifetime.

RESULTS AND DISCUSSION

Solid-state quantum dot-sensitized solar cells (ss-QDSSCs) were fabricated with spiro-OMeTAD as the solid-state HTM and CdS QDs grown by 6 SILAR deposition cycles as the sensitizer, as optimized in previous work.[15]

TiO_2/Al_2O_3/QD Device Performance. One factor limiting efficiencies of QDSSCs is low surface coverage of QDs on the TiO_2,[37,38] which leaves bare TiO_2 surface areas at which recombination can easily occur via direct contact with spiro-OMeTAD. To reduce this major recombination pathway, barrier layers of Al_2O_3 were deposited on the TiO_2 surface prior to QD deposition, in an analogous configuration to that employed in DSSCs. The J−V curves of the resulting TiO_2/Al_2O_3/QD devices under illumination and in the dark are shown in Figure 2. The Al_2O_3 layer suppresses the onset of dark current, as evidenced by the shift with increasing barrier thickness to higher voltage required to extract a given amount of current (Figure 2b). As discussed below in the analysis of the role of the Al_2O_3 layer, the suppression of dark current is attributed to the Al_2O_3 layer providing resistance to electron transfer from TiO_2 to spiro-OMeTAD. Since open-circuit voltage (V_{OC}) is determined by the point at which recombination current fully cancels out photocurrent, the suppression of recombination current would lead to increases in V_{OC}. The observed suppression of dark current with increasing ALD cycles can be taken as an indication of increased resistance to recombination pathways, although dark current is measured when there is no charge in the QDs, unlike recombination current. However, with increasing Al_2O_3 thickness, the photocurrent is attenuated, as seen by the decreasing current density after more than 1 ALD cycle in Figure 2a. At 5 ALD cycles, the loss of photocurrent is so severe that it actually causes a decrease in V_{OC} relative to 3 cycles.

dx.doi.org/10.1021/jp311846r | J. Phys. Chem. C 2013, 117, 5584−5592

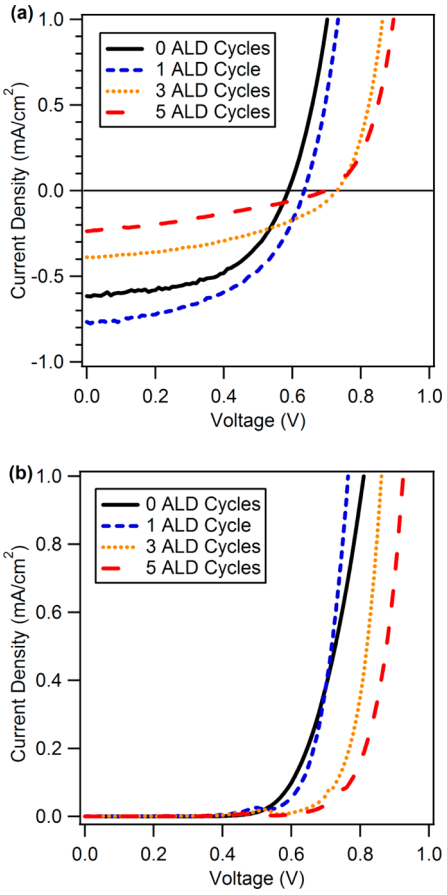

Figure 2. Current density−voltage curves of representative devices in the TiO_2/Al_2O_3/QD configuration with increasing ALD cycles of Al_2O_3 (a) under 1 sun of illumination and (b) in the dark. Al_2O_3 barrier layers are effective at suppressing the onset of dark current, leading to increases in V_{OC}. However, when more than 1 ALD cycle is performed, the Al_2O_3 layer hinders electron injection, thereby reducing J_{SC}.

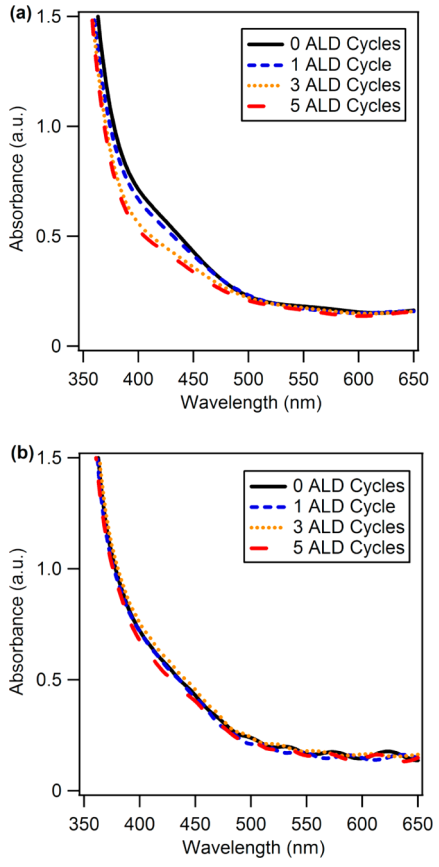

Figure 3. UV−vis absorption spectra of CdS QDs (which begin absorbing at 510 nm) deposited on mesoporous TiO_2 coated with varying ALD cycles of Al_2O_3. For the TiO_2/Al_2O_3/QD configuration (a), the presence of Al_2O_3 reduces CdS growth, but the reduction is not sufficient to fully explain the drops in J_{SC} observed. For the TiO_2/QD/Al_2O_3 configuration (b), no reduction in QD absorption is observed.

For one ALD cycle, the increase in short-circuit current (J_{SC}) seen in Figure 2a is attributed to improved charge collection efficiency, as electrons diffusing through TiO_2 have a better chance of reaching the electrode before recombining. The increases in J_{SC} and V_{OC} at 1 ALD cycle produce a net increase in power conversion efficiency (η), from an average efficiency of 0.18% at 0 ALD cycles to 0.23% at 1 ALD cycle. However, for devices with thicker barrier layers, J_{SC} drops significantly (by 61% after 5 ALD cycles), causing a net decrease in efficiency despite the overall gains in V_{OC}. Part of the drop in current is due to a slight decrease in QD deposition on Al_2O_3-coated TiO_2. UV−vis absorption measurements shown in Figure 3a indicate an ∼20% decrease (calculated from the Beer−Lambert law) in the amount of CdS material deposited on TiO_2 coated with 5 Al_2O_3 ALD cycles, but this does not sufficiently explain the 61% drop in J_{SC}. The high conduction band of Al_2O_3 can inhibit electron injection from the excited QD into TiO_2 if the barrier layer is too thick, causing a drop in current as decay of the excited electron to the ground state in the QD competes with injection. This inhibition of injection accounts for the substantial decreases in J_{SC} at 3 and 5 ALD cycles, which correspond to barrier thicknesses of ∼0.5 and ∼0.8 nm, respectively. In DSSCs, barrier layers of similar thicknesses have been shown to interfere with electron injection.[25,33]

TiO_2/QD/Al_2O_3 Device Performance. Taking advantage of the opportunity in QDSSCs to deposit barrier layers after the TiO_2 has been coated with the sensitizer, TiO_2/QD/Al_2O_3 devices were fabricated. The results (Figure 4) show a similar suppression of the dark current with increasing barrier thickness as observed in TiO_2/Al_2O_3/QD devices, leading to initial gains in V_{OC}.

Notably, a drop in J_{SC} is again observed for barriers thicker than one ALD cycle (Figure 4a). Part of the incentive for the TiO_2/QD/Al_2O_3 configuration is to avoid hindering electron injection into TiO_2, so that gains in V_{OC} can be achieved without decreases in current. Since the drop in J_{SC} cannot be attributed to blocking of electron injection into TiO_2, here, other possible explanations are considered. First, UV−vis absorption measurements (Figure 3b) show that, when deposited after the QDs, the Al_2O_3 layers have no effect on QD absorption, ruling out oxidation or desorption of QDs as potential sources of current loss. Second, it is important to determine whether Al_2O_3 ALD coats the CdS QD surfaces as well as the TiO_2. X-ray photoelectron spectroscopy (XPS) of Al_2O_3 ALD on CdS and TiO_2 films (Figure S1, Supporting Information) confirms that Al_2O_3 grows as readily on CdS as on TiO_2 surfaces, suggesting that the Al_2O_3 is indeed capping the CdS QDs in the mesoporous TiO_2. Thus, the decrease in J_{SC} is attributed to the Al_2O_3 layer preventing regeneration of

dx.doi.org/10.1021/jp311846r | J. Phys. Chem. C 2013, 117, 5584−5592

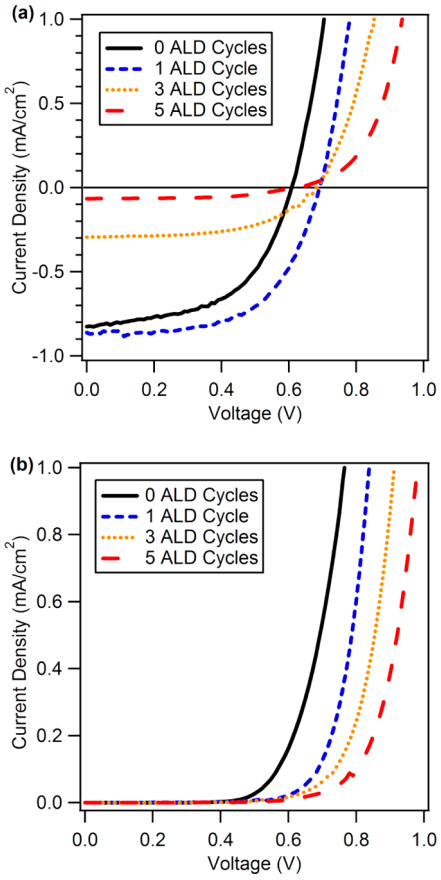

Figure 4. Current density−voltage curves of representative devices in the $TiO_2/QD/Al_2O_3$ configuration increasing ALD cycles of Al_2O_3 (a) under 1 sun of illumination and (b) in the dark. As with the $TiO_2/Al_2O_3/QD$ configuration, the Al_2O_3 layer effectively suppresses dark current but reduces J_{SC} if too thick.

oxidized QDs; that is, the low valence band of Al_2O_3 acts as a tunneling barrier to the transfer of holes from oxidized CdS QDs to spiro-OMeTAD. This conclusion is consistent with recent reports that suggest that regeneration of oxidized QDs is relatively slow compared to dye regeneration in DSSCs, and may be a critical factor in achieving higher efficiencies.[39,40]

Comparison of Layer Placement and Role of Al_2O_3 Layer. Figure 5 provides a comparison of the effect of Al_2O_3 layers on average device parameters in both $TiO_2/Al_2O_3/QD$ and $TiO_2/QD/Al_2O_3$ devices (values are given in Table S1, Supporting Information). The variation in J_{SC} for the control cells (0 ALD cycles), reflects the batch-to-batch variations that cause offsets in J_{SC}, and thus efficiency, for the entire batch of devices (0−5 ALD cycles of a given configuration). However, the relative dependence of J_{SC} on barrier layer thickness within a batch is not affected by these batch-to-batch variations (see discussion of Figure S2, Supporting Information); hence the trends are reliable. Figure 5 shows that qualitatively similar trends in device performance are observed when depositing the Al_2O_3 layer before or after the QDs. Both configurations result in efficiency improvements at one ALD cycle, but at greater cycle numbers, the efficiency decreases, driven by decreases in J_{SC}. These results suggest that the charge separation steps of electron injection to TiO_2 and hole transfer to spiro-OMeTAD are highly dependent on barrier layer thickness. The decrease in J_{SC} at 3 ALD cycles indicates that the barrier layer is thick enough such that there is no longer any kinetic redundancy in the electron injection step, or in the hole transfer to spiro-OMeTAD. In other words, the electron injection or hole transfer steps cannot be slowed down any further without affecting charge collection efficiency.

The efficiency improvements observed for both configurations at one ALD cycle motivated the fabrication of devices in which the mesoporous TiO_2 was treated with 1 Al_2O_3 ALD cycle, followed by CdS QD deposition, and a final 1 Al_2O_3 ALD cycle after the QDs. The resulting $TiO_2/Al_2O_3(1)/QD/Al_2O_3(1)$ devices, where (1) indicates 1 Al_2O_3 ALD cycle, had an average V_{OC} of 0.69 V, which is within error of the V_{OC} enhancement achieved in $TiO_2/QD/Al_2O_3(1)$ devices (0.70 V). An average J_{SC} of 0.81 mA cm^{-2} was observed, leading to an average efficiency of 0.36%. The efficiency of the $TiO_2/Al_2O_3(1)/QD/Al_2O_3(1)$ devices did not exceed those of the $TiO_2/QD/Al_2O_3(1)$ or $TiO_2/Al_2O_3(1)/QD$ devices fabricated within the same batch, although it is comparable to the 0.35% efficiency achieved for $TiO_2/QD/Al_2O_3(1)$ devices in the highest-performing $TiO_2/QD/Al_2O_3$ batch, shown in Figure 5.

In the discussion thus far, we have referred to the Al_2O_3 layers as "barrier layers", implying that the Al_2O_3 layer acts as a tunneling barrier to recombination. The large increases in electron lifetimes with increasing thickness of the Al_2O_3 layer, discussed below, suggest that the Al_2O_3 layer acts primarily as a tunneling barrier, although there may be small contributions from a TiO_2 band shift or passivation of surface defects. We have considered these two other mechanisms by which coating the TiO_2 surface with Al_2O_3 might lead to gains in V_{OC}. In one mechanism, Al_2O_3 acts to passivate the TiO_2 surface, decreasing recombination mediated by TiO_2 surface defects. The successive suppression of the dark current at 3 and 5 ALD cycles (Figure 6) makes a purely surface-mediated effect less likely, although not impossible, as less than a monolayer of Al_2O_3 is deposited in each ALD cycle. Furthermore, in this study, the mesoporous TiO_2 electrodes were coated with a thin layer of TiO_2 deposited by $TiCl_4$ chemical bath treatment, which has been found to improve charge separation in DSSCs, potentially by passivating surface defects on the mesoporous TiO_2.[41] In the second mechanism, the high conduction band of Al_2O_3 could cause an upward shift in the TiO_2 conduction band, increasing the offset between TiO_2 and the highest occupied molecular orbital (HOMO) of spiro-OMeTAD. However, the deposition of Al_2O_3 on mesoporous TiO_2 has been shown to have only minor effects on the TiO_2 conduction band, insufficient to cause the ∼100 mV gains in V_{OC} observed in this work.[42−44] In addition, the increases in electron lifetime measured in this work (Figure 7) are too large to be explained by a conduction band shift.

A comparison of dark current measurements in $TiO_2/Al_2O_3/QD$ versus $TiO_2/QD/Al_2O_3$ devices provides further insight into the role of the Al_2O_3 layer (Figure 6). The suppression of the dark current was quantified by taking the voltage at which the current in a dark $J-V$ curve exceeds a threshold of 0.2 mA cm^{-2}, termed the quantified dark current onset.[25] The current threshold was set relatively low to avoid any effects of variation in series resistance. Unlike V_{OC}, the quantified dark current onset is independent of photocurrent, and thus provides a good metric for comparing the resistance the barrier layer presents to recombination at the interface. Dark current measurements do not replicate the recombination current that occurs in illuminated devices, as the QD layer is not charged in dark conditions, which could affect the charge transfer pathways.

dx.doi.org/10.1021/jp311846r | J. Phys. Chem. C 2013, 117, 5584−5592

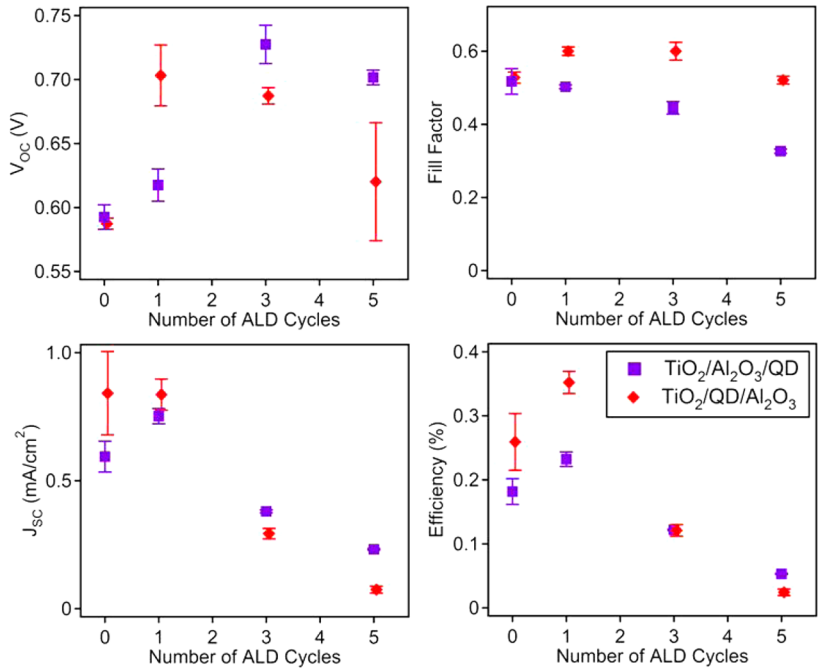

Figure 5. Comparison of device parameters for $TiO_2/Al_2O_3/QD$ and $TiO_2/QD/Al_2O_3$ configurations under 1 sun of illumination with varying ALD cycles of Al_2O_3. Parameters are the average of the top 50% of devices (ranked by efficiency); the set of the top 50% range in number from six to eight devices, and error bars indicate standard deviations. The corresponding values of device parameters are given in Table S1 (Supporting Information). In both configurations, device efficiency improves after 1 ALD cycle of Al_2O_3 but drops thereafter due to decreases in J_{SC}.

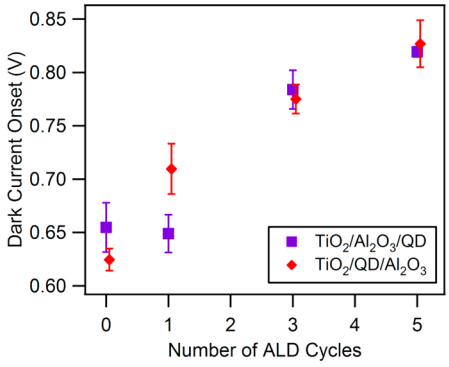

Figure 6. Dark current onset for devices with $TiO_2/Al_2O_3/QD$ and $TiO_2/QD/Al_2O_3$ configurations, with varying ALD cycles of Al_2O_3. The quantified dark current onset is the voltage at which the current of a dark J–V curve reaches a threshold of 0.2 mA/cm^2. Error bars indicate standard deviation. The two configurations show similar suppression of the dark current at thicker Al_2O_3 barrier layers.

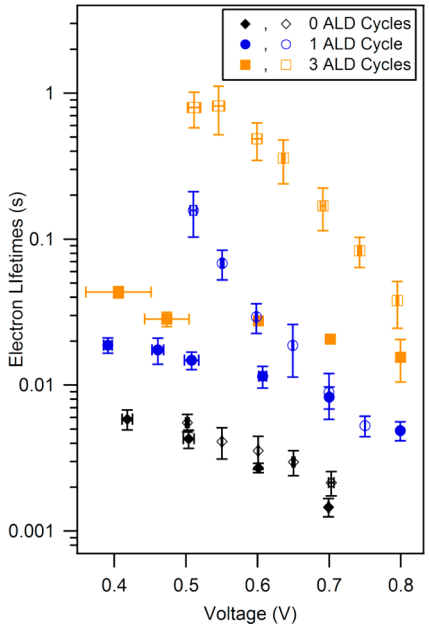

Figure 7. Electron lifetimes for the $TiO_2/Al_2O_3/QD$ (open symbols) and $TiO_2/QD/Al_2O_3$ (closed symbols) as determined via transient photovoltage measurements for varying ALD cycles of Al_2O_3. The larger lifetime improvements achieved with Al_2O_3 barrier layers in the $TiO_2/Al_2O_3/QD$ configuration are attributed to the fact that, in that configuration, recombination to both spiro-OMeTAD and oxidized quantum dots is suppressed.

Dark current consists of electrons traveling through TiO_2 from the transparent electrode toward the interface with spiro-OMeTAD. In dark conditions, the QDs are not oxidized by light absorption, so electrons leaving TiO_2 recombine at the interface with holes traveling through the spiro-OMeTAD phase from the back contact. The more competitive pathway for electrons leaving TiO_2 is through completely bare TiO_2 or TiO_2 surface regions only covered by Al_2O_3, rather than TiO_2 surface areas covered by a QD and an Al_2O_3 layer. This is because tunneling probability decays exponentially with barrier thickness and a surface coating of a QD and an Al_2O_3 layer is thicker than just an Al_2O_3 layer. Consequently, in the $TiO_2/Al_2O_3/QD$ and $TiO_2/QD/Al_2O_3$ devices, the electrons leaving TiO_2 face identical barriers, since the electrons pass through only an Al_2O_3 layer, rather than through the Al_2O_3/QD or QD/Al_2O_3 band structures (which would present different barriers to tunneling). Thus, it is expected that, in the dark, the Al_2O_3 layer suppresses dark current identically for the $TiO_2/Al_2O_3/QD$ and $TiO_2/QD/Al_2O_3$ configurations, as is indeed observed at 3 and 5 ALD cycles (Figure 6). The greater suppression of

dx.doi.org/10.1021/jp311846r | J. Phys. Chem. C 2013, 117, 5584−5592

dark current for the TiO_2/QD/Al_2O_3 devices at the very first ALD cycle, which leads to greater increases in V_{OC} (Figure 5), could be explained by a surface effect in the ALD process. Namely, the SILAR process for the deposition of QDs could potentially increase surface roughness of the TiO_2, leading to increased nucleation of Al_2O_3 for the first ALD cycle in TiO_2/QD/Al_2O_3 devices, and hence a slightly thicker Al_2O_3 recombination layer.

Effect of Al_2O_3 on Electron Lifetimes. Decreases in the rate of recombination at the TiO_2 interface should result in increased electron lifetimes (τ_n) in the TiO_2. To test this, the impact of Al_2O_3 layers on electron lifetime was determined by transient photovoltage measurements of TiO_2/Al_2O_3/QD and TiO_2/QD/Al_2O_3 devices (Figure 7). The observed decrease in electron lifetime with applied bias is well-known for DSSCs, and can be understood by the positive dependence of the recombination rate constant on electron concentration in TiO_2, and the increase in electron concentration with applied bias.[44,45] The electron lifetime values for the control case of 0 ALD cycles are similar to those previously reported in 2 μm thick solid-state DSSCs employing spiro-OMeTAD as the HTM.[46] As shown in Figure 7, we found that increasing the Al_2O_3 layer thickness leads to substantial improvements in electron lifetimes, supporting the conclusion that the Al_2O_3 layer acts as a tunneling barrier to electron recombination.

The difference between electron lifetime improvements in TiO_2/Al_2O_3/QD versus TiO_2/QD/Al_2O_3 devices indicates that, under illumination (transient photovoltage measurements are taken at 1 sun illumination), the CdS QDs do participate in recombination. The TiO_2/Al_2O_3/QD configuration results in the greatest enhancement of electron lifetimes. This is attributed to the ability of TiO_2/Al_2O_3/QD devices to block both recombination to oxidized QDs and to spiro-OMeTAD, while the TiO_2/QD/Al_2O_3 configuration only blocks recombination to spiro-OMeTAD (shown schematically in Figure 1). In addition, the Al_2O_3 layer in TiO_2/QD/Al_2O_3 devices may interfere with regeneration of oxidized QDs by spiro-OMeTAD, leading to an increase in the concentration of oxidized QDs at a given time. This, in turn, could increase recombination to oxidized QDs, and thus partially offset the benefits (i.e., increased electron lifetimes) of decreased recombination with spiro-OMeTAD.

The slope of $\log(\tau_n)$ versus voltage depends on the exponential coefficient of the density of localized states in TiO_2 (which increases exponentially with energy level), as well as the exact dependence of the recombination rate constant, $k_n = 1/\tau_n$, on the electron concentration.[44,47] Therefore, the higher slope observed in TiO_2/Al_2O_3/QD devices compared to the TiO_2/QD/Al_2O_3 devices could suggest a difference in the rate constant's dependence on electron density, consistent with different recombination pathways at work in the different configurations. However, the difference in slope could also be due to a lower capacitance at the interface in the TiO_2/Al_2O_3/QD devices.

That the TiO_2/Al_2O_3/QD configuration yields the greatest improvements in electron lifetimes further suggests that recombination of TiO_2 electrons through defects on the QD outer surface is not the limiting factor in achieving high electron lifetimes. Here, defects on the QD outer surface refers to sites on the QD surface facing spiro-OMeTAD, not the QD interface with TiO_2. If the dominant recombination pathway *were* defects on the QD outer surface, we would expect TiO_2/QD/Al_2O_3 devices with the Al_2O_3 layer passivating the QD surface to show the greatest increases in electron lifetimes. This assessment is based on the assumption that any impact the TiO_2/Al_2O_3/QD barrier configuration might have on this QD outer surface defect recombination (by increasing the separation between the TiO_2 and QDs) would be minimal compared to the TiO_2/QD/Al_2O_3 barrier configuration, which directly passivates QD surface defects.

In summary, these results demonstrate the ability of Al_2O_3 barrier layers to greatly enhance electron lifetimes and suggest that recombination to both spiro-OMeTAD and oxidized QDs plays a role in limiting electron lifetimes. Overall, the effectiveness of Al_2O_3 layers as a barrier to recombination leads us to propose a route to capturing the benefits of enhanced V_{OC} without losses in current. Specifically, deposition of barrier layers after QDs could be modified to allow for selective deposition only on bare TiO_2 surfaces, such that the layer is not coating the QD surface. This could be achieved by material choice of a barrier layer that grows selectively on the TiO_2, or by masking the QD surface with a removable organic surface layer. In this geometry, the barrier layer would prevent the recombination of electrons in TiO_2 to holes in spiro-OMeTAD, without obstructing electron injection into TiO_2 or regeneration of the oxidized QD by hole transfer to spiro-OMeTAD. Decreasing the rate of recombination (thus increasing electron lifetimes and diffusion lengths) enables the use of thicker active layers in solid-state devices and the potential for substantial gains in efficiency from increased absorption. Furthermore, solving the problem of recombination in QD-sensitized devices is particularly attractive, as the higher temperature stability of QDs, compared to dyes, provides the opportunity to deposit the hole transport material by melt infiltration, thus addressing the other challenge of moving to thicker active layers, that of insufficient pore-filling of the solid-state HTM.[22,34]

■ CONCLUSIONS

Solid-state CdS QDSSCs were fabricated with Al_2O_3 barrier layers deposited by ALD. The Al_2O_3 layer was found to act primarily as a tunneling barrier to electron recombination, resulting in a suppression of the dark current and substantial increases in electron lifetimes in TiO_2. Both TiO_2/Al_2O_3/QD and TiO_2/QD/Al_2O_3 configurations resulted in the same qualitative trends in device performance with increasing barrier layer thickness. Namely, V_{OC} initially increases with a concomitant increase in efficiency before the barrier layer begins at greater thicknesses to interfere with charge-transfer steps necessary for photocurrent collection, resulting in drops in efficiency. That drops in J_{SC} with increased barrier thickness were observed in both barrier configurations suggests that both electron injection to TiO_2 and hole transfer to spiro-OMeTAD are sensitive to the presence of tunneling barriers. A comparison of the TiO_2/Al_2O_3/QD and TiO_2/QD/Al_2O_3 barrier layer configurations' impact on dark current and electron lifetimes indicates that electron transfer from TiO_2 to spiro-OMeTAD is a major source of recombination, though the back transfer of TiO_2 electrons to oxidized QDs also has the potential to limit electron lifetimes, particularly when regeneration of oxidized QDs is inhibited by a barrier layer capping the QD, as in the TiO_2/QD/Al_2O_3 configuration.

■ ASSOCIATED CONTENT

Supporting Information

Table of average device parameter values plotted in Figure 5, X-ray photoelectron spectroscopy characterization of growth of Al_2O_3 deposited by ALD on CdS versus TiO_2 planar substrates, and analysis of consistency of device parameter trends across different batches of devices. This material is available free of charge via the Internet at http://pubs.acs.org.

■ AUTHOR INFORMATION

Corresponding Author

*E-mail: sbent@stanford.edu. Tel: 1 650 723-0385. Fax: 1 650 723-9780.

Notes

The authors declare no competing financial interest.

■ ACKNOWLEDGMENTS

This publication was based on work supported by the Center for Advanced Molecular Photovoltaics (Award No. KUS-C1-015-21), made by King Abdullah University of Science and Technology (KAUST). We would like to thank the Stanford Nanocharacterization Laboratory (SNL) staff for their support. The ALD reactor and process development for these studies were carried out with support by the Center for Nanostructuring for Efficient Energy Conversion, an Energy Frontier Research Center (EFRC) funded by the U.S. Department of Energy, Office of Basic Energy Sciences, Award No. DE-SC0001060.

■ REFERENCES

(1) O'Regan, B.; Grätzel, M. A Low-Cost, High-Efficiency Solar Cell Based on Dye-Sensitized Colloidal TiO_2 Films. *Nature* **1991**, *353*, 737−740.

(2) Yella, A.; Lee, H.-W.; Tsao, H. N.; Yi, C.; Chandiran, A. K.; Nazeeruddin, M. K.; Diau, E. W.-G.; Yeh, C.-Y.; Zakeeruddin, S. M.; Grätzel, M. Porphyrin-Sensitized Solar Cells with Cobalt (I^-/I_3^-)-Based Redox Electrolyte Exceed 12% Efficiency. *Science* **2011**, *334*, 629−634.

(3) Nozik, A. J. Quantum Dot Solar Cells. *Physica E* **2002**, *14*, 115−120.

(4) Kamat, P. V. Quantum Dot Solar Cells: Semiconductor Nanocrystals as Light Harvesters. *J. Phys. Chem. C* **2008**, *112*, 18737−18753.

(5) Mora-Seró, I.; Bisquert, J. Breakthroughs in the Development of Semiconductor-Sensitized Solar Cells. *J. Phys. Chem. Lett.* **2010**, *1*, 3046−3052.

(6) Rühle, S.; Shalom, M.; Zaban, A. Quantum-Dot-Sensitized Solar Cells. *ChemPhysChem* **2010**, *11*, 2290−2304.

(7) Plass, R.; Pelet, S.; Krueger, J.; Grätzel, M.; Bach, U. Quantum Dot Sensitization of Organic/Inorganic Hybrid Solar Cells. *J. Phys. Chem. B* **2002**, *106*, 7578−7580.

(8) Shen, Q.; Arae, D.; Toyoda, T. Photosensitization of Nanostructured TiO_2 with CdSe Quantum Dots: Effects of Microstructure and Electron Transport in TiO_2 Substrates. *J. Photochem. Photobiol., A* **2004**, *164*, 75−80.

(9) Weller, H. Quantized Semiconductor Particles: A Novel State of Matter for Materials Science. *Adv. Mater.* **1993**, *5*, 88−95.

(10) Peter, L. M. The Grätzel Cell: Where Next? *J. Phys. Chem. Lett.* **2011**, *2*, 1861−1867.

(11) Moreels, I.; Lambert, K.; Smeets, D.; De Muynck, D.; Nollet, T.; Martins, J.; Vanhaecke, F.; Vantomme, A.; Delerue, C.; Allan, G.; et al. Size-Dependent Optical Properties of Colloidal PbS Quantum Dots. *ACS Nano* **2009**, *3*, 3023−3030.

(12) Diguna, L. J.; Shen, Q.; Kobayashi, J.; Toyoda, T. High Efficiency of CdSe Quantum-Dot-Sensitized TiO_2 Inverse Opal Solar Cells. *Appl. Phys. Lett.* **2007**, *91*, 023116−023113.

(13) Niitsoo, O.; Sarkar, S. K.; Pejoux, C.; Rühle, S.; Cahen, D.; Hodes, G. Chemical Bath Deposited CdS/CdSe-Sensitized Porous TiO_2 Solar Cells. *J. Photochem. Photobiol., A* **2006**, *181*, 306−313.

(14) Baker, D. R.; Kamat, P. V. Photosensitization of TiO_2 Nanostructures with CdS Quantum Dots: Particulate Versus Tubular Support Architectures. *Adv. Funct. Mater.* **2009**, *19*, 805−811.

(15) Ardalan, P.; Brennan, T. P.; Lee, H.-B.-R.; Bakke, J. R.; Ding, I. K.; McGehee, M. D.; Bent, S. F. Effects of Self-Assembled Monolayers on Solid-State CdS Quantum Dot Sensitized Solar Cells. *ACS Nano* **2011**, *5*, 1495−1504.

(16) Lévy-Clément, C.; Tena-Zaera, R.; Ryan, M. A.; Katty, A.; Hodes, G. CdSe-Sensitized p-CuSCN/Nanowire n-ZnO Heterojunctions. *Adv. Mater.* **2005**, *17*, 1512−1515.

(17) Brennan, T. P.; Ardalan, P.; Lee, H.-B.-R.; Bakke, J. R.; Ding, I. K.; McGehee, M. D.; Bent, S. F. Atomic Layer Deposition of CdS Quantum Dots for Solid-State Quantum Dot Sensitized Solar Cells. *Adv. Energy Mater.* **2011**, *1*, 1169−1175.

(18) Dasgupta, N. P.; Jung, H. J.; Trejo, O.; McDowell, M. T.; Hryciw, A.; Brongersma, M.; Sinclair, R.; Prinz, F. B. Atomic Layer Deposition of Lead Sulfide Quantum Dots on Nanowire Surfaces. *Nano Lett.* **2011**, *11*, 934−940.

(19) Bach, U.; Lupo, D.; Comte, P.; Moser, J. E.; Weissortel, F.; Salbeck, J.; Spreitzer, H.; Grätzel, M. Solid-State Dye-Sensitized Mesoporous TiO_2 Solar Cells with High Photon-to-Electron Conversion Efficiencies. *Nature* **1998**, *395*, 583−585.

(20) Kron, G.; Egerter, T.; Werner, J. H.; Rau, U. Electronic Transport in Dye-Sensitized Nanoporous TiO_2 Solar Cells: Comparison of Electrolyte and Solid-State Devices. *J. Phys. Chem. B* **2003**, *107*, 3556−3564.

(21) Snaith, H. J.; Schmidt-Mende, L. Advances in Liquid-Electrolyte and Solid-State Dye-Sensitized Solar Cells. *Adv. Mater.* **2007**, *19*, 3187−3200.

(22) Ding, I. K.; Tétreault, N.; Brillet, J.; Hardin, B. E.; Smith, E. H.; Rosenthal, S. J.; Sauvage, F.; Grätzel, M.; McGehee, M. D. Pore-Filling of Spiro-OMeTAD in Solid-State Dye Sensitized Solar Cells: Quantification, Mechanism, and Consequences for Device Performance. *Adv. Funct. Mater.* **2009**, *19*, 2431−2436.

(23) Melas-Kyriazi, J.; Ding, I. K.; Marchioro, A.; Punzi, A.; Hardin, B. E.; Burkhard, G. F.; Tétreault, N.; Grätzel, M.; Moser, J.-E.; McGehee, M. D. The Effect of Hole Transport Material Pore Filling on Photovoltaic Performance in Solid-State Dye-Sensitized Solar Cells. *Adv. Energy Mater.* **2011**, *1*, 407−414.

(24) Bakke, J. R.; Pickrahn, K. L.; Brennan, T. P.; Bent, S. F. Nanoengineering and Interfacial Engineering of Photovoltaics by Atomic Layer Deposition. *Nanoscale* **2011**, *3*, 3482−3508.

(25) Brennan, T. P.; Bakke, J. R.; Ding, I. K.; Hardin, B. E.; Nguyen, W. H.; Mondal, R.; Bailie, C. D.; Margulis, G. Y.; Hoke, E. T.; Sellinger, A.; et al. The Importance of Dye Chemistry and $TiCl_4$ Surface Treatment in the Behavior of Al_2O_3 Recombination Barrier Layers Deposited by Atomic Layer Deposition in Solid-State Dye-Sensitized Solar Cells. *Phys. Chem. Chem. Phys.* **2012**, *14*, 12130−12140.

(26) Son, H.-J.; Wang, X.; Prasittichai, C.; Jeong, N. C.; Aaltonen, T.; Gordon, R. G.; Hupp, J. T. Glass-Encapsulated Light Harvesters: More Efficient Dye-Sensitized Solar Cells by Deposition of Self-Aligned, Conformal, and Self-Limited Silica Layers. *J. Am. Chem. Soc.* **2012**, *134*, 9537−9540.

(27) Hod, I.; González-Pedro, V.; Tachan, Z.; Fabregat-Santiago, F.; Mora-Seró, I. n.; Bisquert, J.; Zaban, A. Dye Versus Quantum Dots in Sensitized Solar Cells: Participation of Quantum Dot Absorber in the Recombination Process. *J. Phys. Chem. Lett.* **2011**, *2*, 3032−3035.

(28) Shalom, M.; Dor, S.; Rühle, S.; Grinis, L.; Zaban, A. Core/CdS Quantum Dot/Shell Mesoporous Solar Cells with Improved Stability and Efficiency Using an Amorphous TiO_2 Coating. *J. Phys. Chem. C* **2009**, *113*, 3895−3898.

(29) Shen, Q.; Kobayashi, J.; Diguna, L. J.; Toyoda, T. Effect of ZnS Coating on the Photovoltaic Properties of CdSe Quantum Dot-Sensitized Solar Cells. *J. Appl. Phys.* **2008**, *103*, 084304−084305.
(30) Choi, H.; Nicolaescu, R.; Paek, S.; Ko, J.; Kamat, P. V. Supersensitization of CdS Quantum Dots with a Near-Infrared Organic Dye: Toward the Design of Panchromatic Hybrid-Sensitized Solar Cells. *ACS Nano* **2011**, *5*, 9238−9245.
(31) Haque, S. A.; Palomares, E.; Cho, B. M.; Green, A. N. M.; Hirata, N.; Klug, D. R.; Durrant, J. R. Charge Separation Versus Recombination in Dye-Sensitized Nanocrystalline Solar Cells: The Minimization of Kinetic Redundancy. *J. Am. Chem. Soc.* **2005**, *127*, 3456−3462.
(32) Mäkinen, V.; Honkala, K.; Häkkinen, H. Atomic Layer Deposition of Aluminum Oxide on TiO_2 and Its Impact on N3 Dye Adsorption from First Principles. *J. Phys. Chem. C* **2011**, *115*, 9250−9259.
(33) Lin, C.; Tsai, F.-Y.; Lee, M.-H.; Lee, C.-H.; Tien, T.-C.; Wang, L.-P.; Tsai, S.-Y. Enhanced Performance of Dye-Sensitized Solar Cells by an Al_2O_3 Charge-Recombination Barrier Formed by Low-Temperature Atomic Layer Deposition. *J. Mater. Chem.* **2009**, *19*, 2999−3003.
(34) Leijtens, T.; Ding, I. K.; Giovenzana, T.; Bloking, J. T.; McGehee, M. D.; Sellinger, A. Hole Transport Materials with Low Glass Transition Temperatures and High Solubility for Application in Solid-State Dye-Sensitized Solar Cells. *ACS Nano* **2012**, *6*, 1455−1462.
(35) Spanhel, L.; Haase, M.; Weller, H.; Henglein, A. Photochemistry of Colloidal Semiconductors. 20. Surface Modification and Stability of Strong Luminescing CdS Particles. *J. Am. Chem. Soc.* **1987**, *109*, 5649−5655.
(36) Snaith, H. J.; Humphry-Baker, R.; Chen, P.; Cesar, I.; Zakeeruddin, S. M.; Grätzel, M. Charge Collection and Pore Filling in Solid-State Dye-Sensitized Solar Cells. *Nanotechnology* **2008**, *19*, 424003.
(37) Shen, H.; Lin, H.; Liu, Y.; Li, J.; Oron, D. Study of Quantum Dot/Inorganic Layer/Dye Molecule Sandwich Structure for Electrochemical Solar Cells. *J. Phys. Chem. C* **2012**, *116*, 15185−15191.
(38) Lee, H.; Wang, M.; Chen, P.; Gamelin, D. R.; Zakeeruddin, S. M.; Grätzel, M.; Nazeeruddin, M. K. Efficient CdSe Quantum Dot-Sensitized Solar Cells Prepared by an Improved Successive Ionic Layer Adsorption and Reaction Process. *Nano Lett.* **2009**, *9*, 4221−4227.
(39) Zewdu, T.; Clifford, J. N.; Hernandez, J. P.; Palomares, E. Photo-Induced Charge Transfer Dynamics in Efficient TiO_2/CdS/CdSe Sensitized Solar Cells. *Energy Environ. Sci.* **2011**, *4*, 4633−4638.
(40) Martinez-Ferrero, E.; Sero, I. M.; Albero, J.; Gimenez, S.; Bisquert, J.; Palomares, E. Charge Transfer Kinetics in CdSe Quantum Dot Sensitized Solar Cells. *Phys. Chem. Chem. Phys.* **2010**, *12*, 2819−2821.
(41) O'Regan, B. C.; Durrant, J. R.; Sommeling, P. M.; Bakker, N. J. Influence of the $TiCl_4$ Treatment on Nanocrystalline TiO_2 Films in Dye-Sensitized Solar Cells: Charge Density, Band Edge Shifts, and Quantification of Recombination Losses at Short Circuit. *J. Phys. Chem. C* **2007**, *111*, 14001−14010.
(42) Ondersma, J. W.; Hamann, T. W. Impedance Investigation of Dye-Sensitized Solar Cells Employing Outer-Sphere Redox Shuttles. *J. Phys. Chem. C* **2010**, *114*, 638−645.
(43) Antila, L. J.; Heikkilä, M. J.; Mäkinen, V.; Humalamäki, N.; Laitinen, M.; Linko, V.; Jalkanen, P.; Toppari, J.; Aumanen, V.; Kemell, M.; et al. ALD Grown Aluminum Oxide Submonolayers in Dye-Sensitized Solar Cells: The Effect on Interfacial Electron Transfer and Performance. *J. Phys. Chem. C* **2011**, *115*, 16720−16729.
(44) O'Regan, B. C.; Scully, S.; Mayer, A. C.; Palomares, E.; Durrant, J. The Effect of Al_2O_3 Barrier Layers in TiO_2/Dye/CuSCN Photovoltaic Cells Explored by Recombination and DOS Characterization Using Transient Photovoltage Measurements. *J. Phys. Chem. B* **2005**, *109*, 4616−4623.
(45) van de Lagemaat, J.; Park, N. G.; Frank, A. J. Influence of Electrical Potential Distribution, Charge Transport, and Recombination on the Photopotential and Photocurrent Conversion Efficiency of Dye-Sensitized Nanocrystalline TiO_2 Solar Cells: A Study by Electrical Impedance and Optical Modulation Techniques. *J. Phys. Chem. B* **2000**, *104*, 2044−2052.
(46) Snaith, H. J.; Grätzel, M. Electron and Hole Transport through Mesoporous TiO_2 Infiltrated with Spiro-MeOTAD. *Adv. Mater.* **2007**, *19*, 3643−3647.
(47) Bisquert, J.; Fabregat-Santiago, F.; Mora-Seró, I.; Garcia-Belmonte, G.; Giménez, S. Electron Lifetime in Dye-Sensitized Solar Cells: Theory and Interpretation of Measurements. *J. Phys. Chem. C* **2009**, *113*, 17278−17290.